Electronic supplementary information for

Tuning the memristive behaviors of electropolymerized metallopolymers via metal core

Lingyun Shen,[ab*] Jing Li,[ab] Yongfang Li,[ab] Chenyang Hu,[a] Zhiqiang Sun[a] and Xuan Pang[ab]

[a]*State Key Laboratory of Polymer Science and Technology, Changchun Institute of Applied Chemistry, Chinese Academy of Sciences, Changchun 130022, China. E-mail: lyshen@ciac.ac.cn*

[b]*School of Applied Chemistry and Engineering, University of Science and Technology of China, Hefei 230026, China.*

Table of Contents

1. Supplemental Figures and Notes

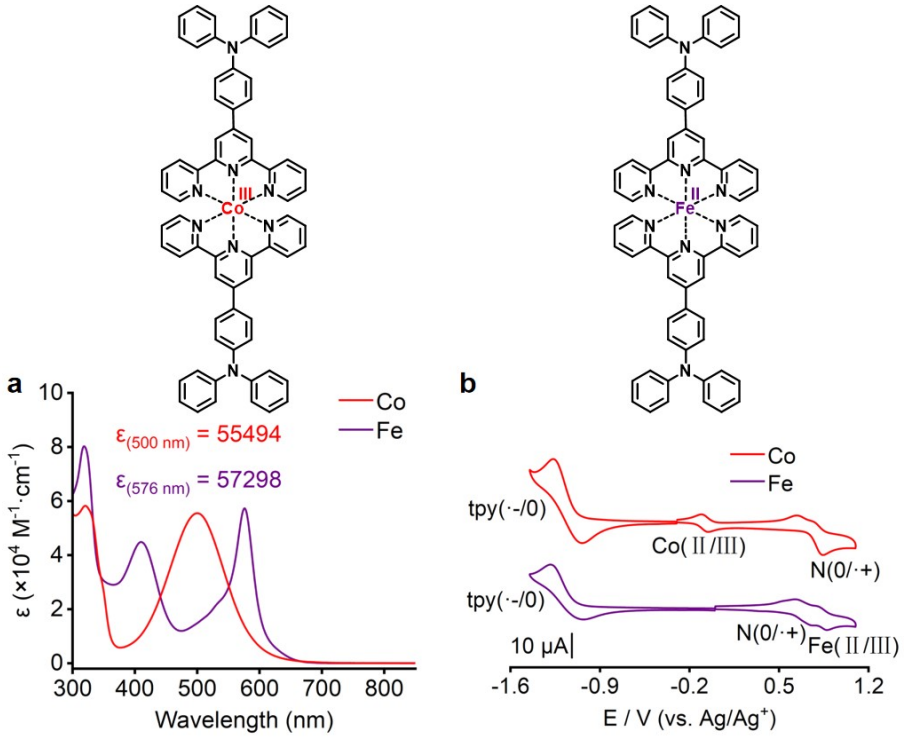

Fig. S1 (a) Ultraviolet-visible (UV-Vis) absorption spectra of the Co and Fe monomers in CH_3CN. (b) Cyclic voltammetry (CV) of 0.2 mM monomers in 0.1 M n-Bu_4NClO_4 CH_3CN solution at a scan rate of 100 mV/s using glassy carbon electrodes. The absorption peak at 500 nm of the Co monomer is attributed to the ligand-to-metal charge transfer (LMCT) transition[1]. The absorption peak at 576 nm of the Fe monomer is attributed to the metal-to-ligand charge transfer (MLCT) transition[2]. The Co monomer exhibit extra metal-centered reduction in contrast to the Fe counterpart.

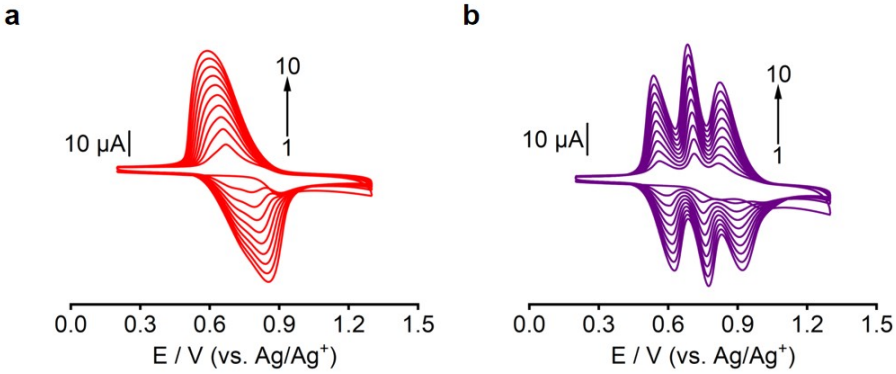

Fig. S2 Successive 10 cycles CV of 0.2 mM Co (a) and Fe (b) monomers in 0.1 M n-Bu_4NClO_4 CH_2Cl_2 solution at a scan rate of 100 mV/s using glassy carbon electrodes.

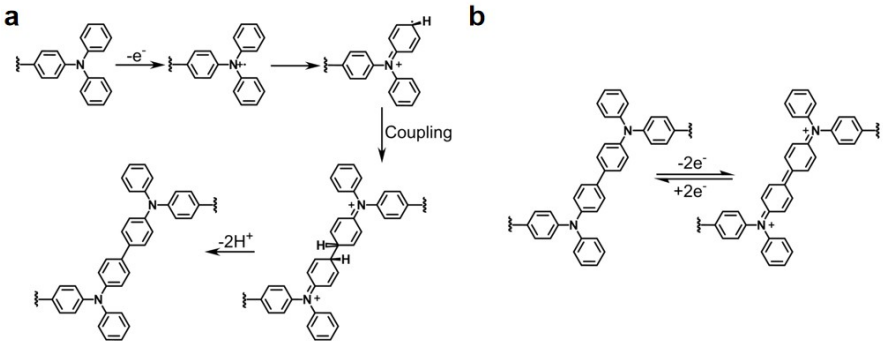

Fig. S3 (a) Illustration of the dimerization of triphenylamine radical cations to form tetraphenylbenzidine upon electrochemical oxidation. (b)

Illustration of the reversible redox of the coupling product tetraphenylbenzidine. Upon oxidation, tetraphenylbenzidine forms a stable resonance structure and does not undergo further coupling reactions.

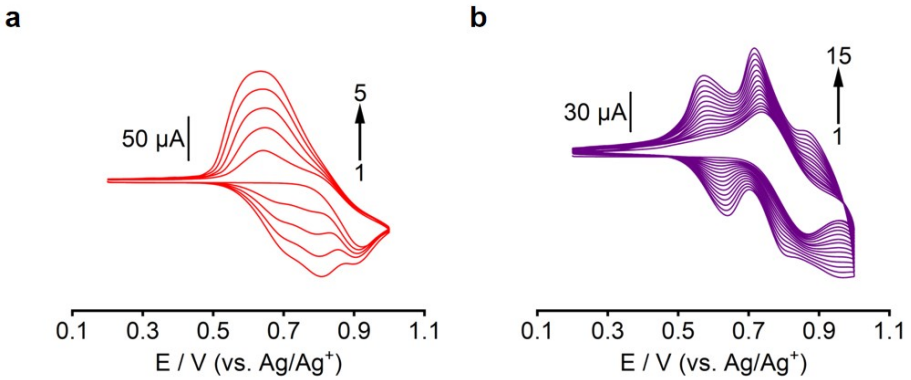

Fig. S4 Electropolymerization performed by scanning 1–5 and 3–15 cycles (in increments of 1 and 3 cycles, respectively) of 0.2 mM Co (a) and Fe (b) monomers in 0.1 M n-Bu_4NClO_4 CH_2Cl_2 solution at a scan rate of 50 mV/s on indium-tin oxide (ITO) glass electrodes.

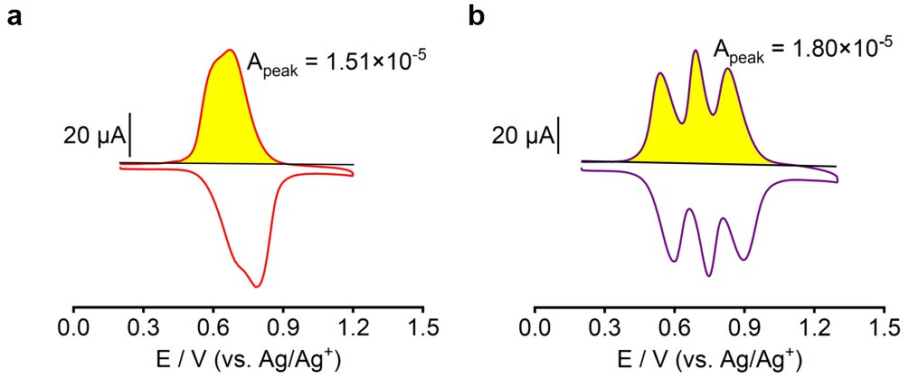

Fig. S5 Illustrations for surface coverage (Γ) calculation from the intergration of Co1 (a) and Fe3 (b) metallopolymers' CV using the formula $\Gamma = \frac{10A_{peak}}{nFA}$. n = 2 (Co metallopolymers) or 3 (Fe metallopolymers), F = 96485.33 C/mol, A = 2 cm^2.

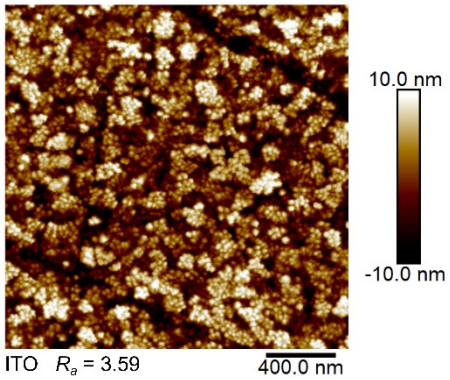

Fig. S6 Atomic force microscopy (AFM) height images of the ITO substrate with a size of 2.0 × 2.0 μm.

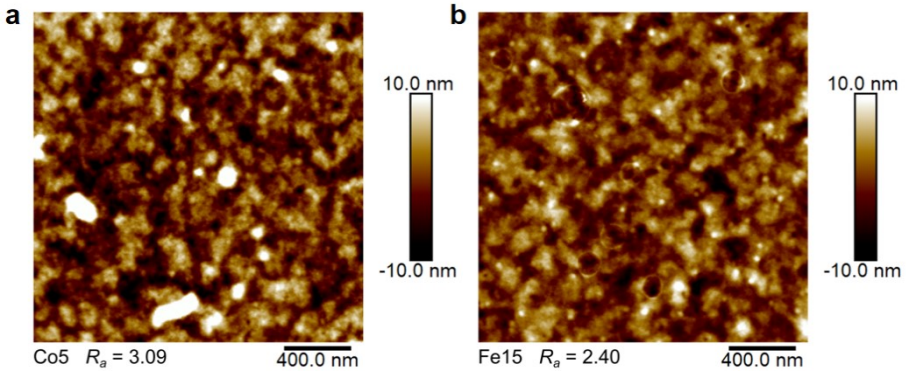

Fig. S7 AFM height images of the Co5 (a) and Fe15 (b) metallopolymers with a size of 2.0 × 2.0 μm.

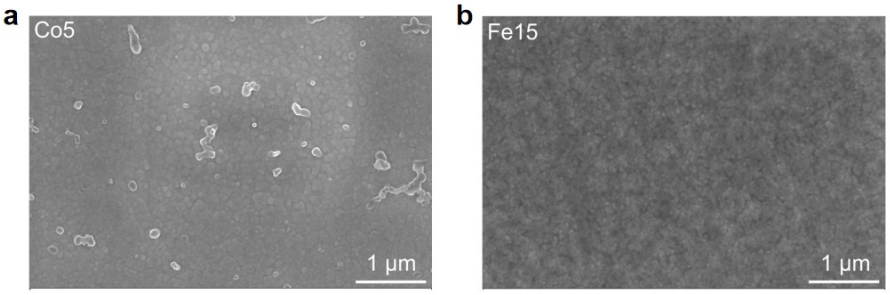

Fig. S8 Scanning electron microscopy (SEM) images of the Co5 (a) and Fe15 (b) metallopolymers.

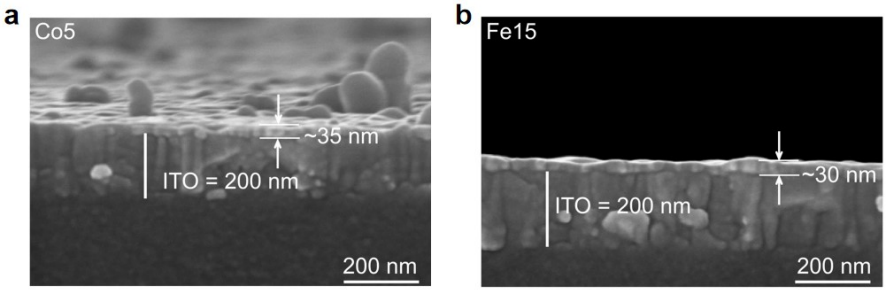

Fig. S9 SEM cross-section images of the Co5 (a) and Fe15 (b) metallopolymers.

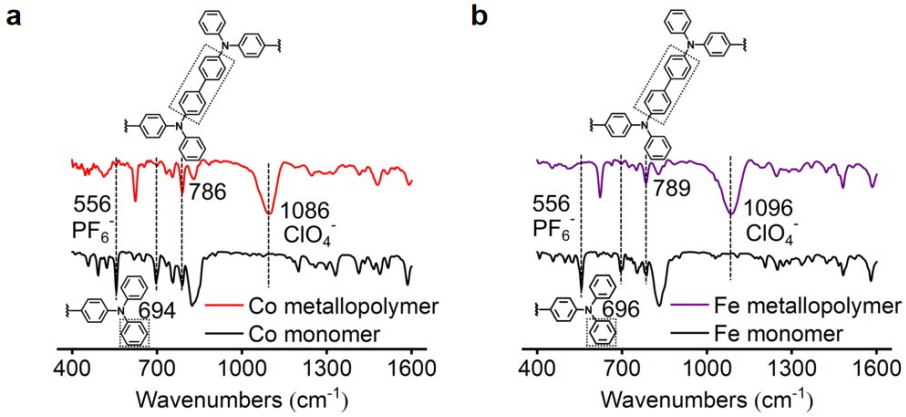

Fig. S10 Normalized infrared reflection absorption spectra (IR-RAS) of the Co, Fe metallopolymers and corresponding monomers. The vibration peak at 694 cm^{-1} and 696 cm^{-1} relative to the mono-substituted benzene rings of triphenylamine weakens after electropolymerization. The vibration peak at 786 cm^{-1} and 789 cm^{-1} relative to the di-substituted benzene rings raises in metallopolymers[3]. The vibration peak at 556 cm^{-1} attributed to PF_6^- disappears in metallopolymers. The vibration peak at 1086 cm^{-1} and 1098 cm^{-1} relative to ClO_4^- emerges in metallopolymers[4].

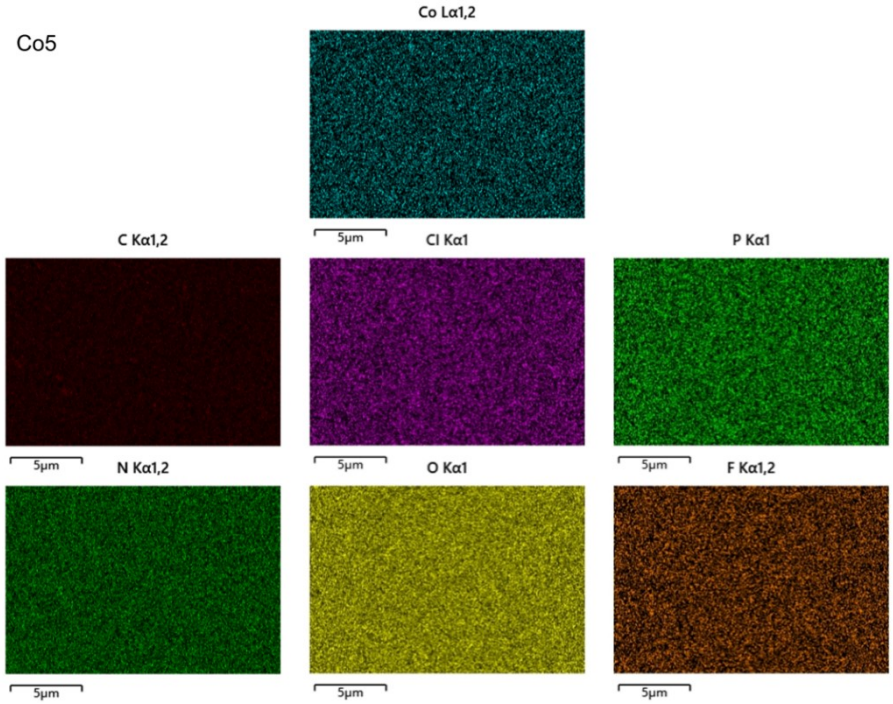

Fig. S11 SEM mapping images of key elements in the Co5 metallopolymer. These images show the uniformity of the electropolymerized Co metallopolymer, avoiding short circuits during memristive tests.

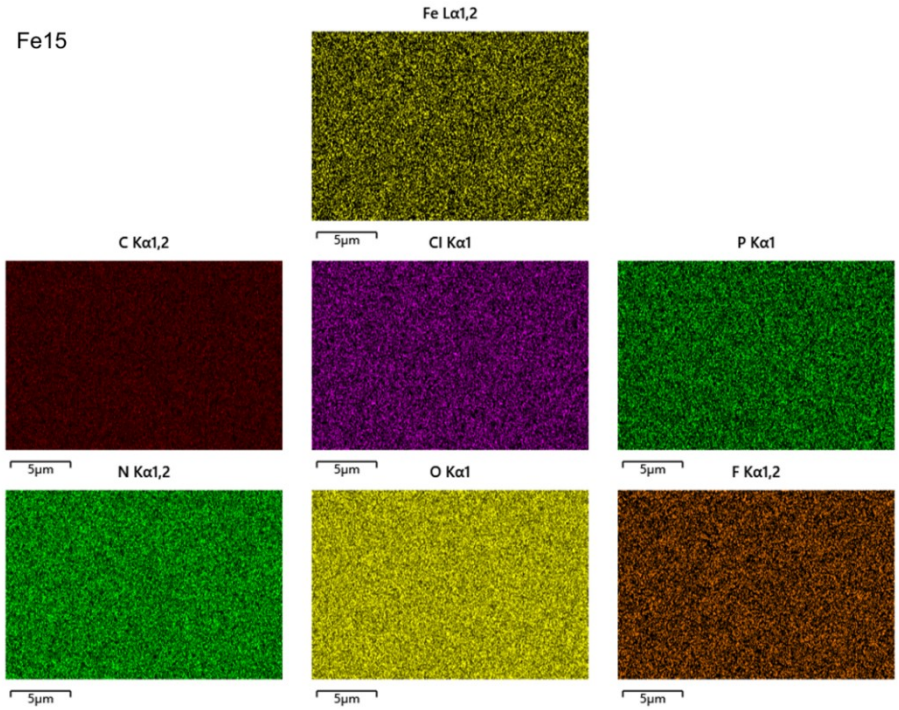

Fig. S12 SEM mapping images of key elements in the Fe15 metallopolymer. These images show the uniformity of the electropolymerized Fe metallopolymer, avoiding short circuits during memristive tests.

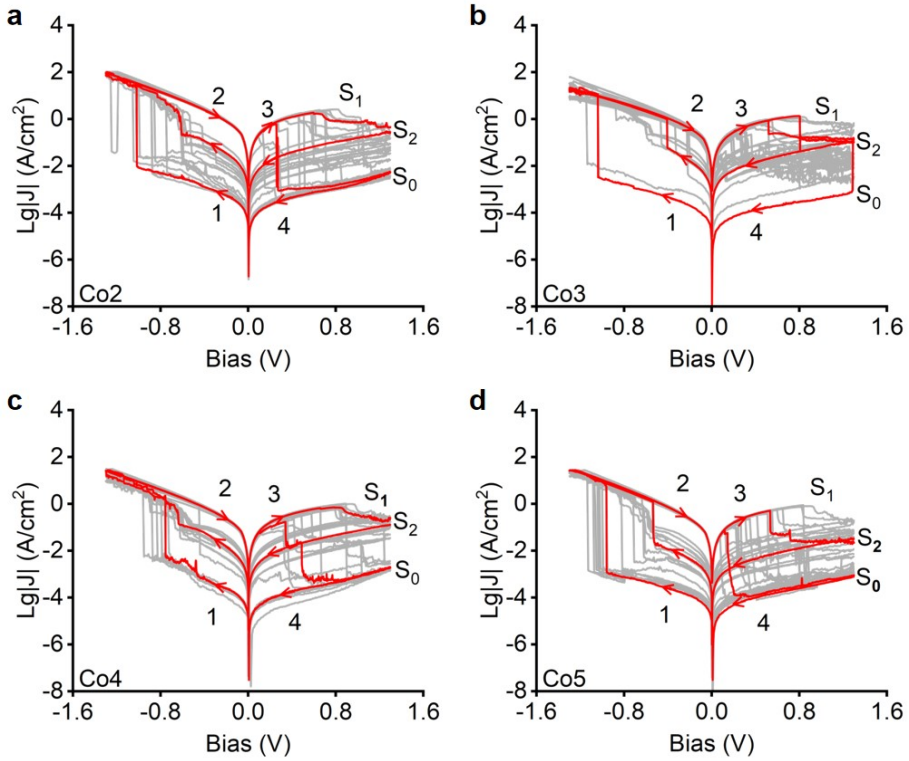

Fig. S13 *J–V* curves of the Co2 (a), Co3 (b), Co4 (c) and Co5 (d) metallopolymers at a bias range of ±1.3 V with a scan rate of 500 mV/s.

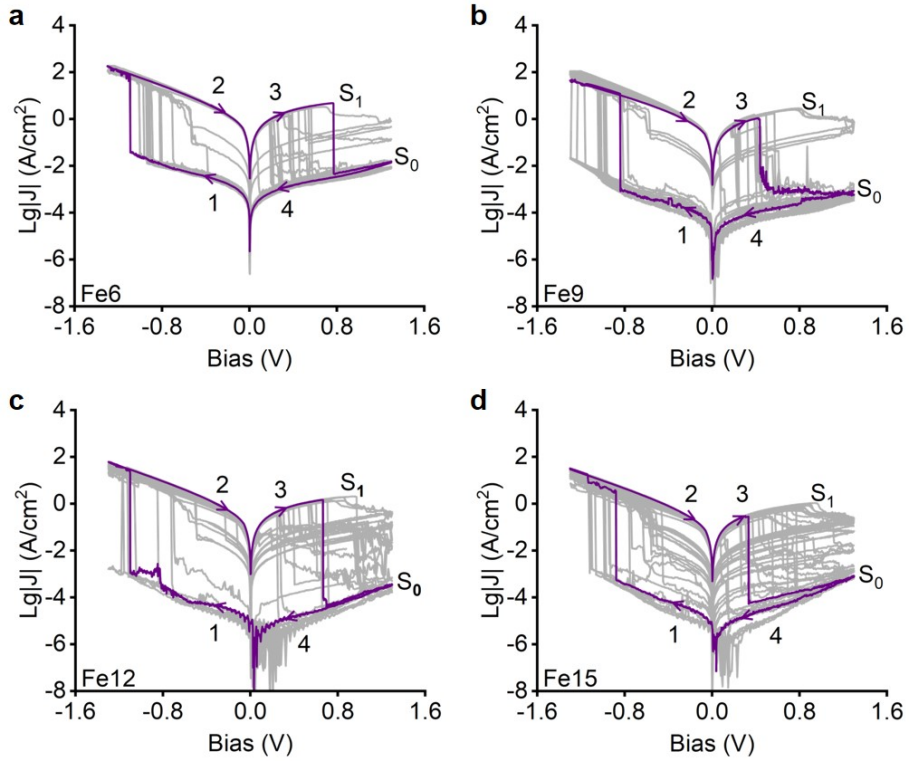

Fig. S14 *J–V* curves of the Fe6 (a), Fe9 (b), Fe12 (c) and Fe15 (d) metallopolymers at a bias range of ±1.3 V with a scan rate of 500 mV/s.

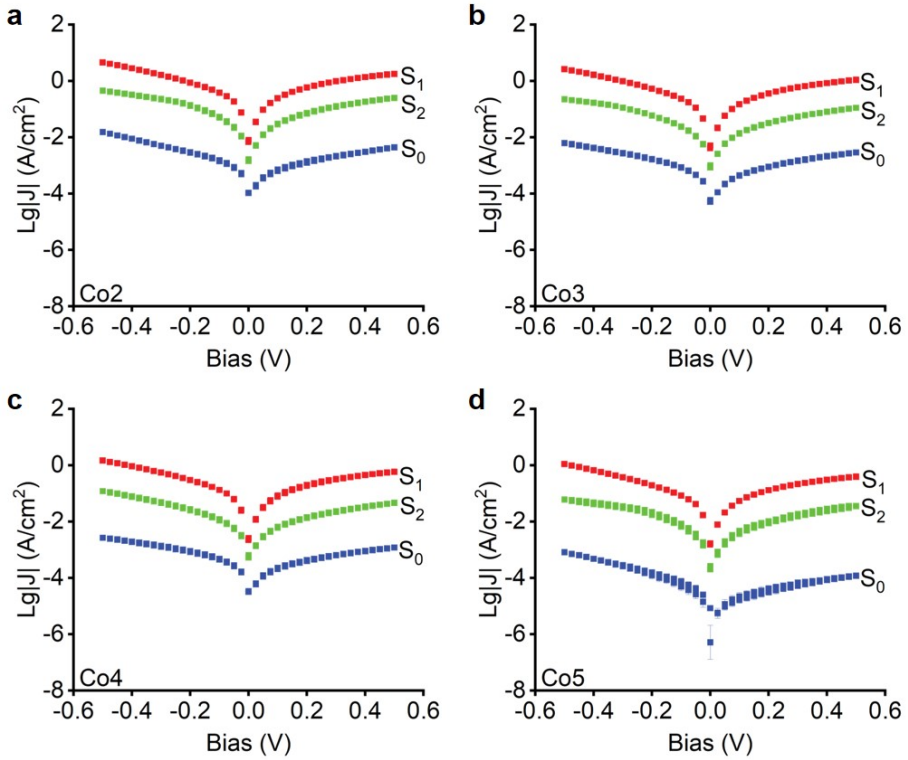

Fig. S15 *J–V* scatterplots of the Co2 (a), Co3 (b), Co4 (c) and Co5 (d) metallopolymers in different resistance states at a bias range of ±0.5 V. Each curve is a statistical result of dozens of cycles.

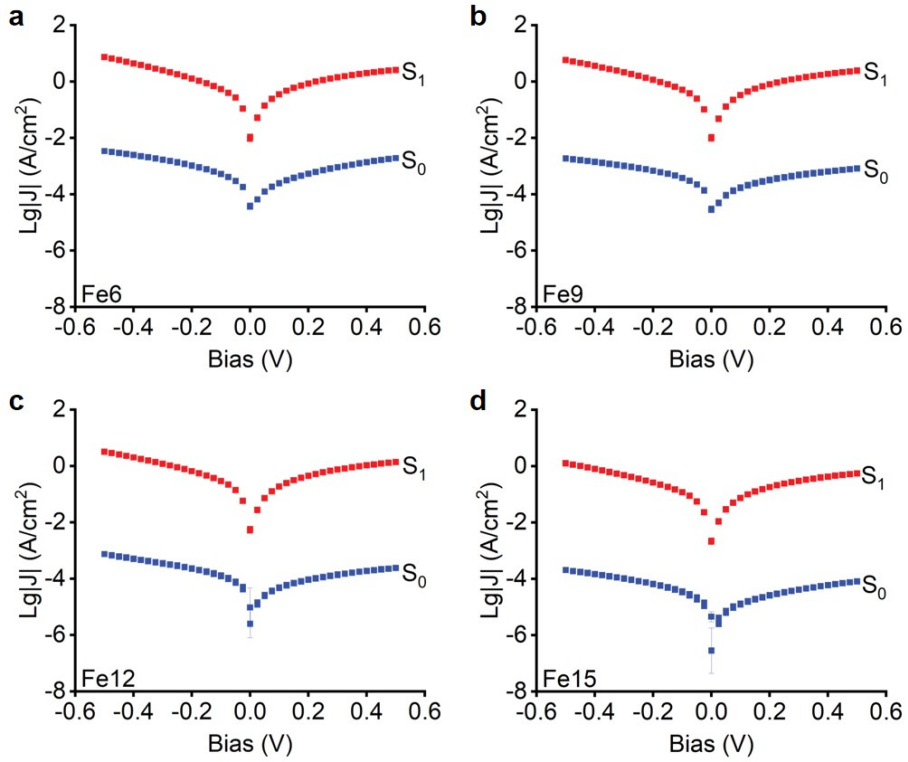

Fig. S16 *J–V* scatterplots of the Fe6 (a), Fe9 (b), Fe12 (c) and Fe15 (d) metallopolymers in different resistance states at a bias range of ±0.5 V. Each curve is a statistical result of dozens of cycles.

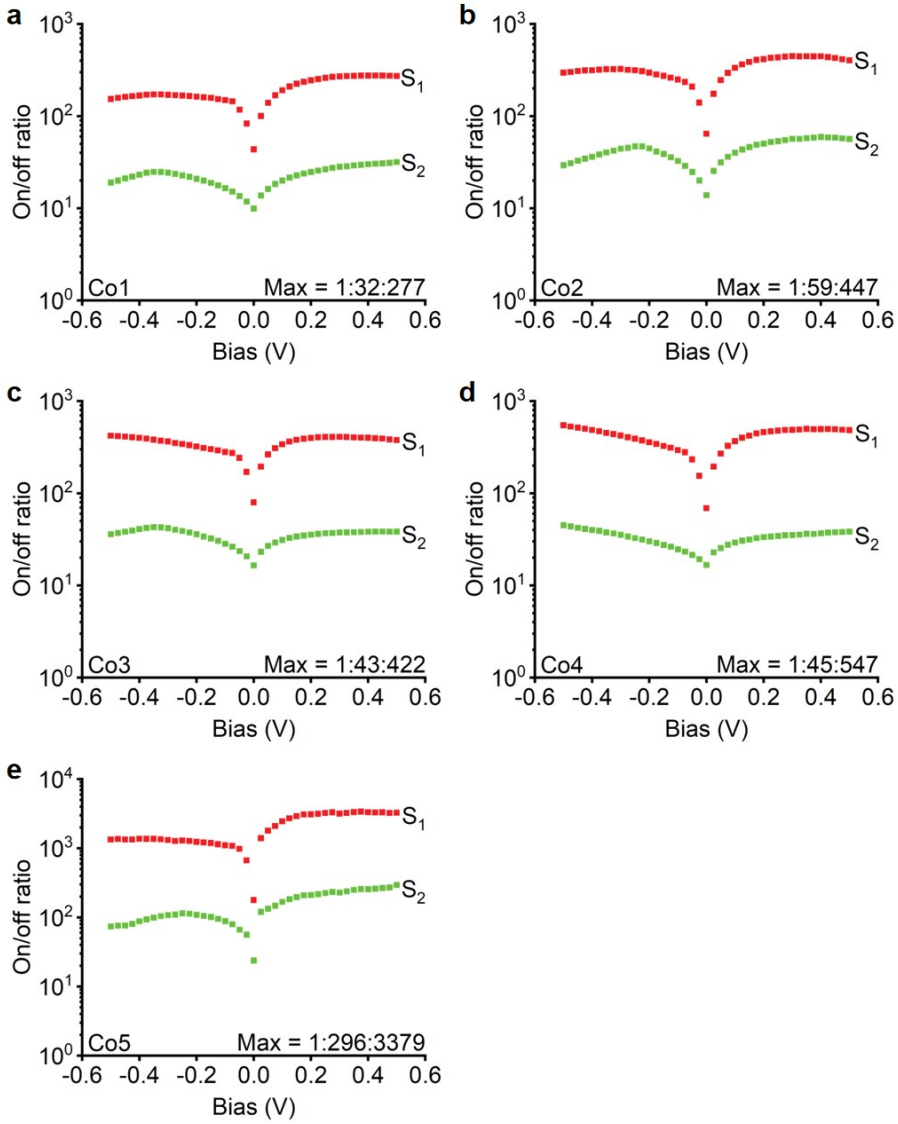

Fig. S17 The on/off ratio scatterplots of the Co1 (a), Co2 (b), Co3 (c), Co4 (d), and Co5 (e) metallopolymers in different resistance states at a bias range of ±0.5 V.

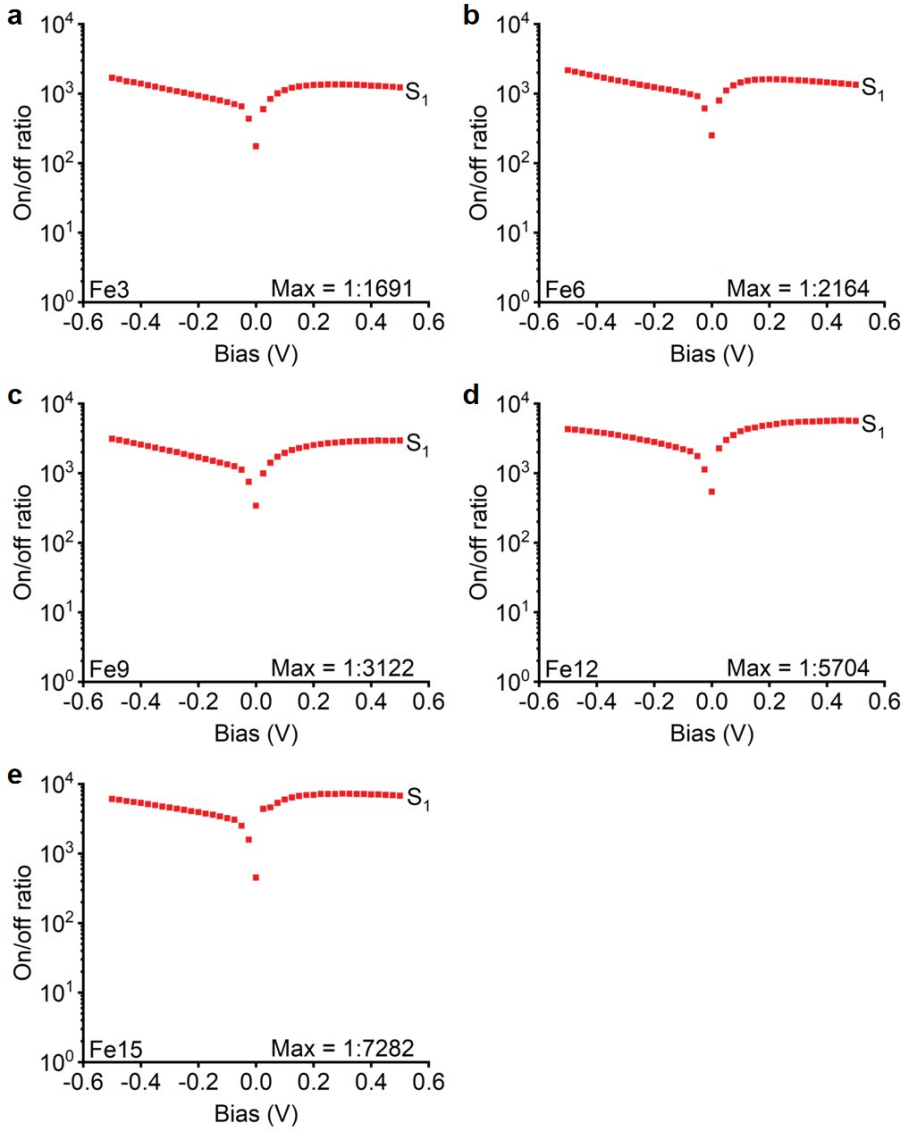

Fig. S18 The on/off ratio scatterplots of the Fe3 (a), Fe6 (b), Fe9 (c), Fe12 (d), and Fe15 (e) metallopolymers in different resistance states at a bias range of ±0.5 V.

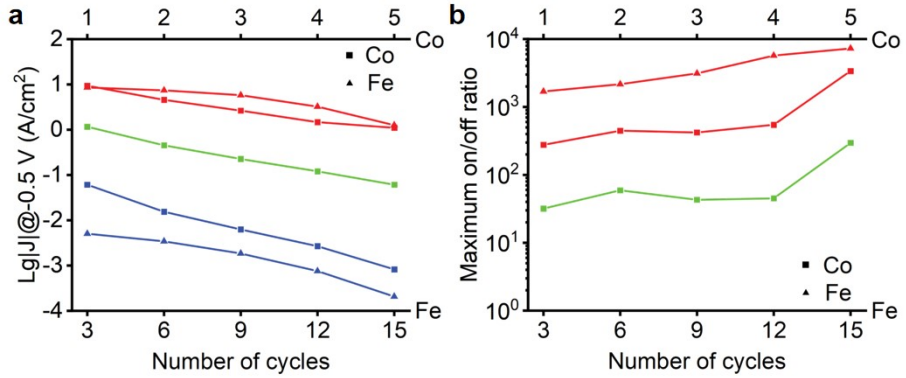

Fig. S19 Dependence of the current density (a) and on/off ratio (b) on the thickness of two metallopolymers.

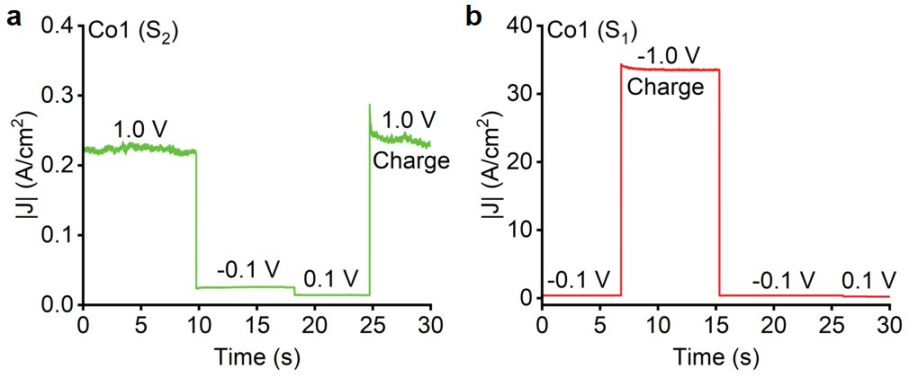

Fig. S20 *J–T* curves of the Co1 metallopolymer in the S_2 (a) and S_1 (b). The charge behavior occurs after switching to a high bias, while the discharge behavior is absent.

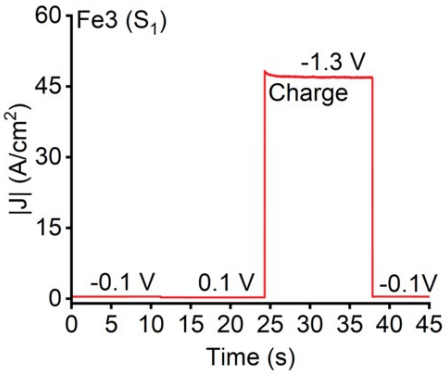

Fig. S21 *J–T* curve of the Fe3 metallopolymer in the S_1. The charge behavior occurs after switching to a high bias, while the discharge behavior is absent.

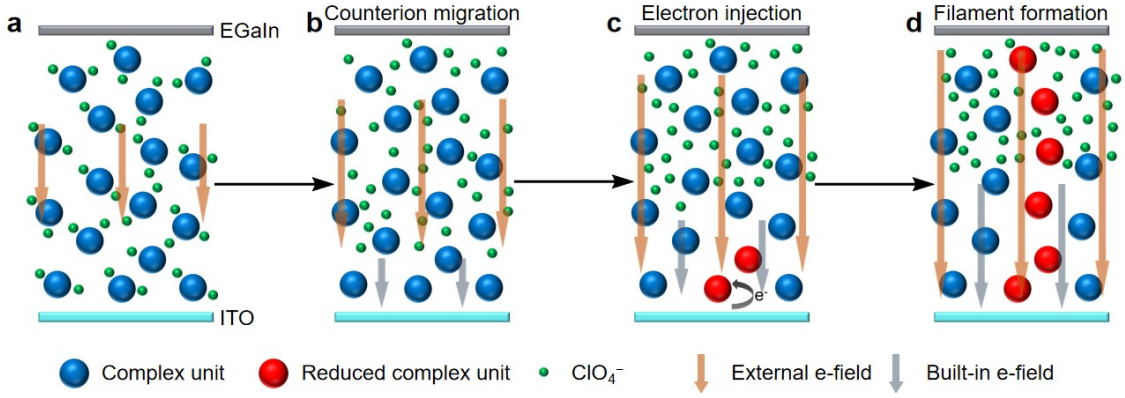

Fig. S22 Schematic diagram of the resistive switching mechanism with the metallopolymer backbone undrawn for clarity. (a) Initially, the external electric field is insufficient to overcome the ionic bonds, so counterions randomly distribute around the complex unit. (b) When the external electric field becomes large enough, the counterions migrate to form a built-in electric field, which enhances the interfacial electric field near the electrode surface. (c) When the interfacial electric field is high enough, additional electrons are injected and subsequently reduce the complex units. (d) The reduced complex units form filaments with enhanced conductivity, which results from the incorporation of additional electrons.

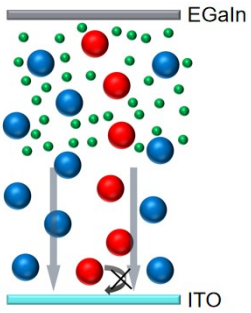

Fig. S23 Schematic diagram of the non-volatility mechanism. When the external electric field is removed the locked counterion distribution sustains the residual interfacial electric field, which prevents the injected electrons from being released.

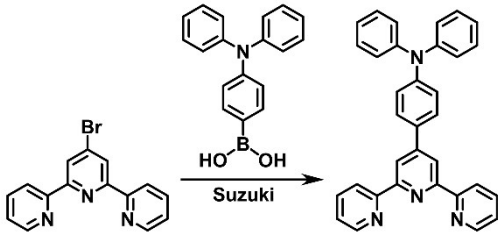

Fig. S24 Synthesis route of the ligand 4'-(4-(diphenylamino)phenyl)-[2,2':6',2"]terpyridine.

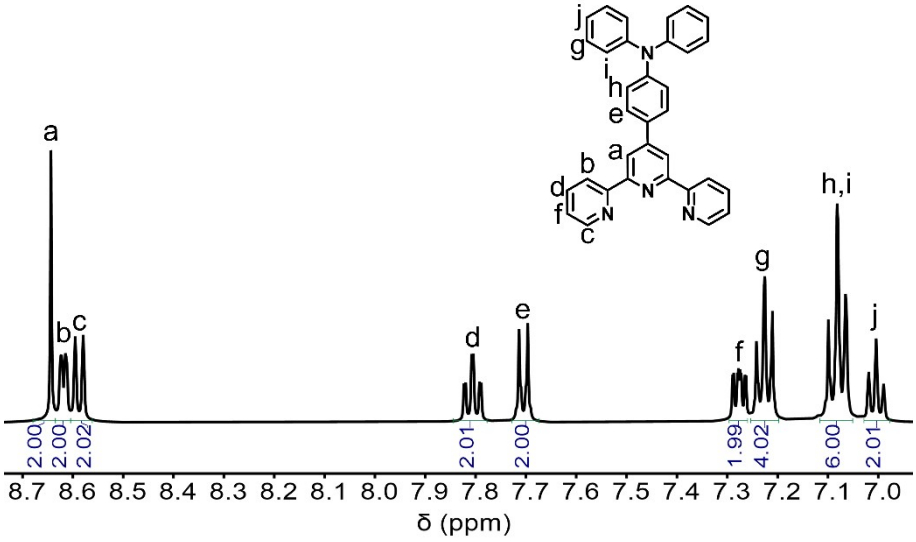

Fig. S25 ^{1}H nuclear magnetic resonance (NMR) spectrum of the ligand 4'-(4-(diphenylamino)phenyl)-[2,2':6',2"]terpyridine in CD_2Cl_2

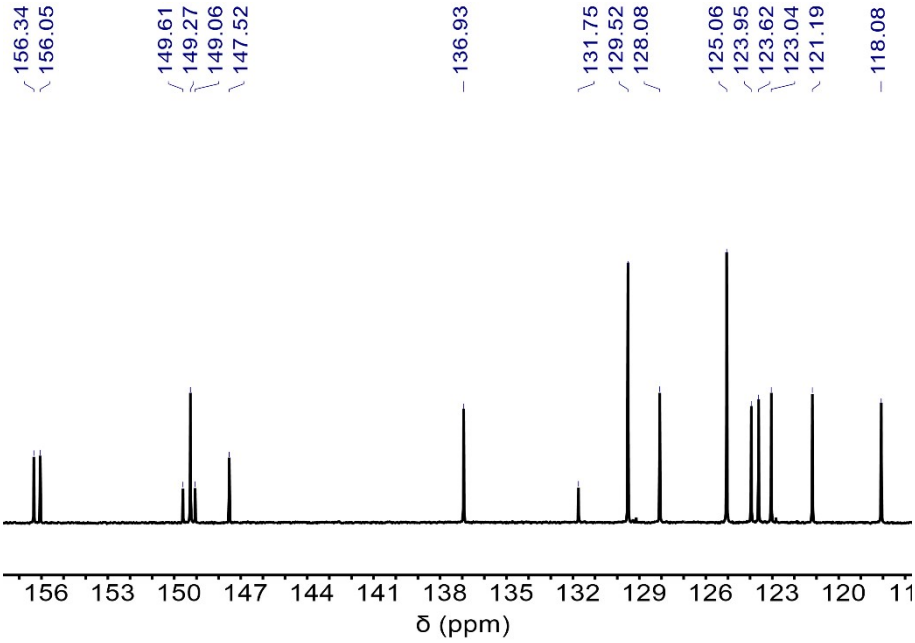

Fig. S26 ^{13}C NMR spectrum of the ligand 4'-(4-(diphenylamino)phenyl)-[2,2':6',2"]terpyridine in CD_2Cl_2.

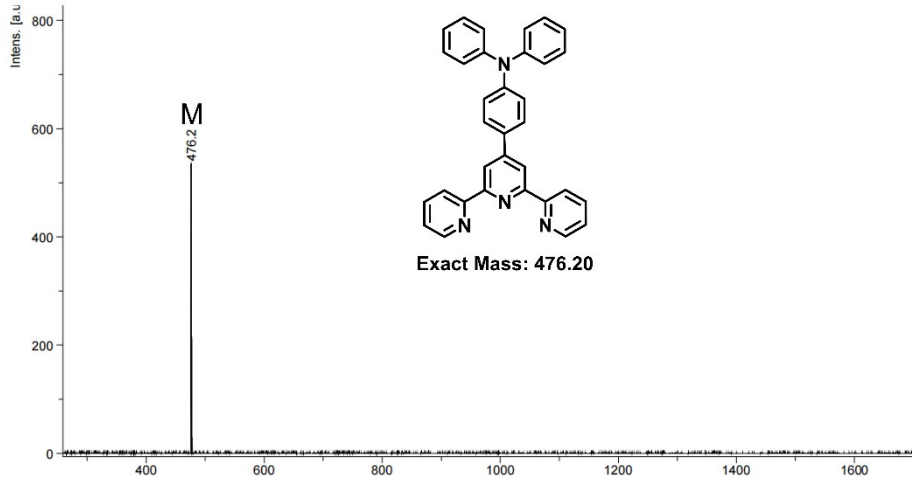

Fig. S27 MALDI-TOF mass spectrum of the ligand 4'-(4-(diphenylamino)phenyl)-[2,2':6',2"]terpyridine in CH_2Cl_2.

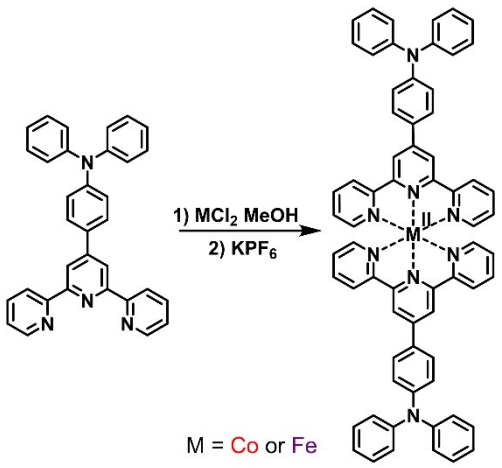

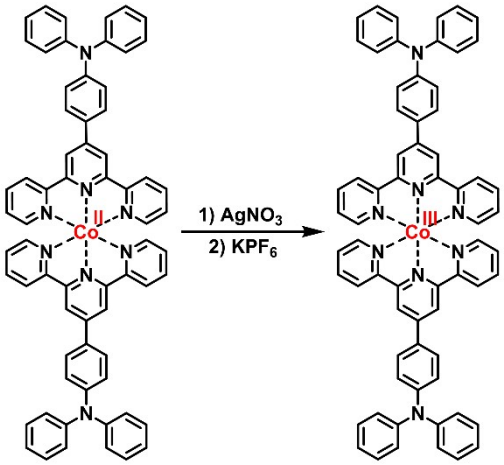

Fig. S28 Synthesis route of the Co and Fe monomers.

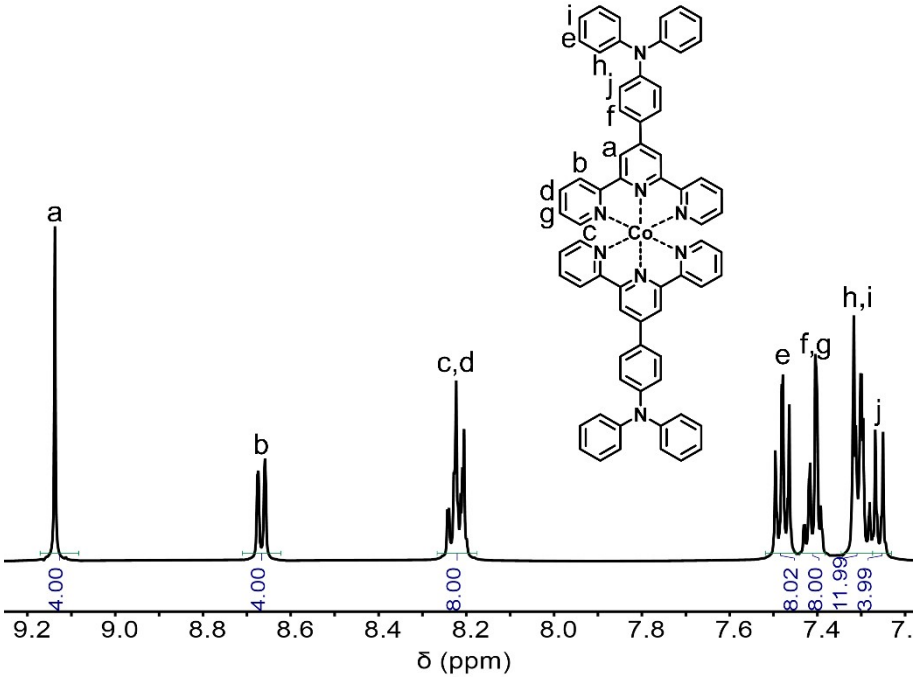

Fig. S29 ^{1}H NMR spectrum of the Co monomer in CD_3CN.

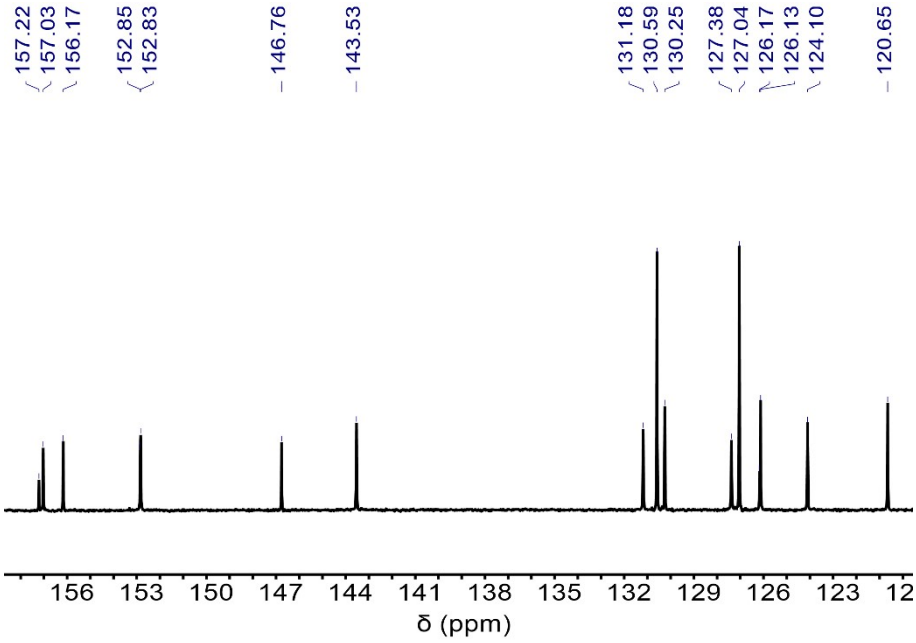

Fig. S30 ^{13}C NMR spectrum of the Co monomer in CD_3CN.

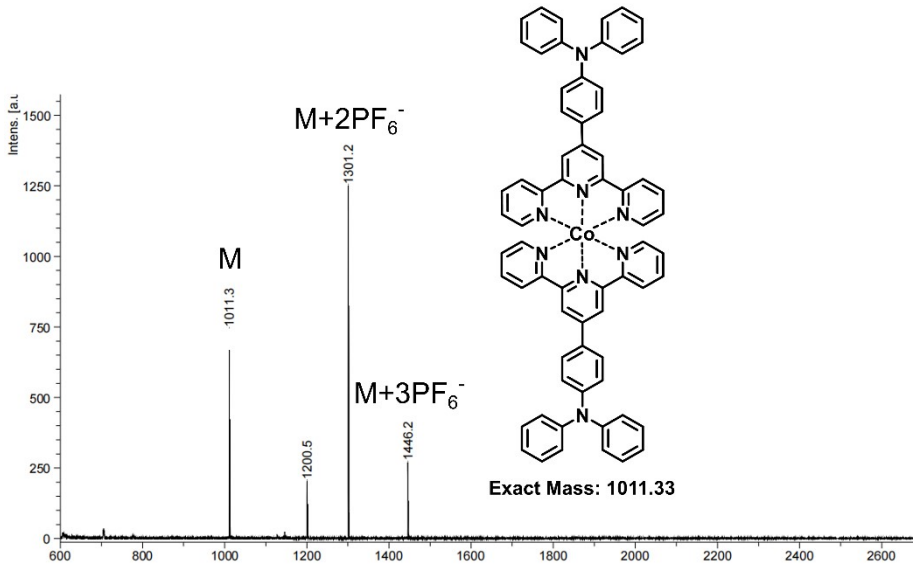

Fig. S31 MALDI-TOF mass spectrum of the Co monomer in CH_3CN.

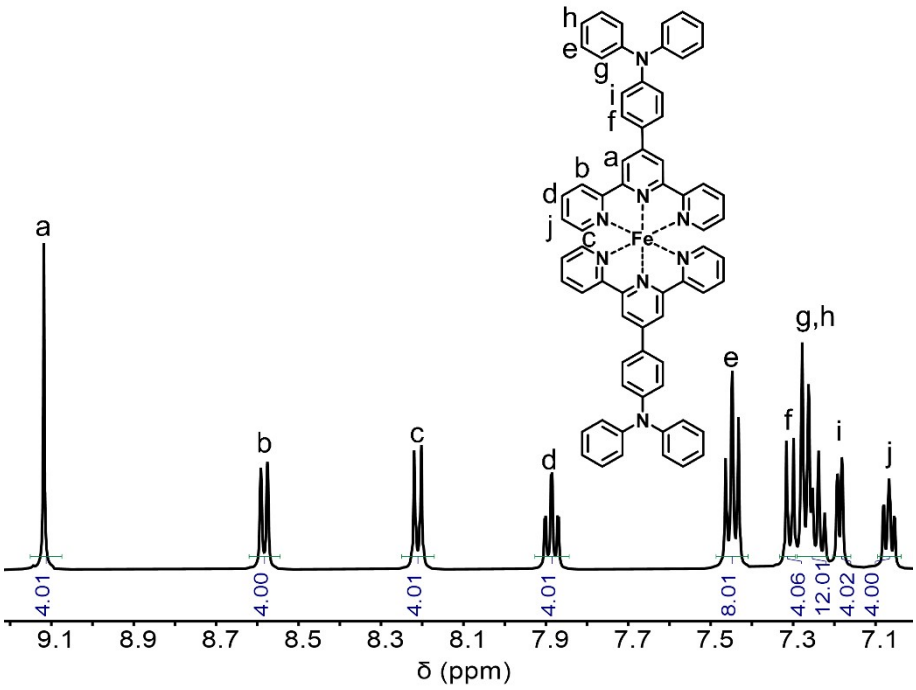

Fig. S32 ^{1}H NMR spectrum of the Fe monomer in CD_3CN.

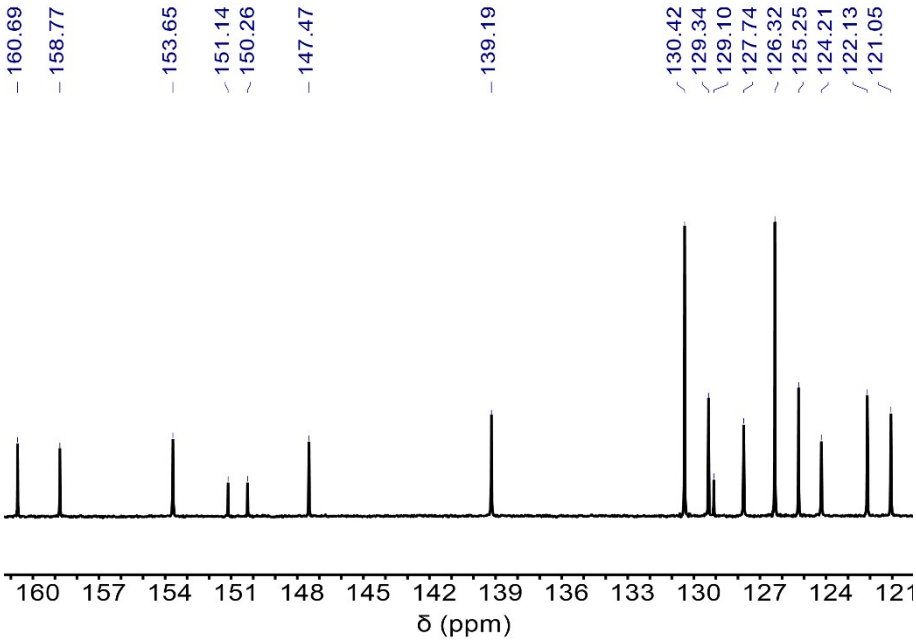

Fig. S33 ^{13}C NMR spectrum of the Fe monomer in CD_3CN.

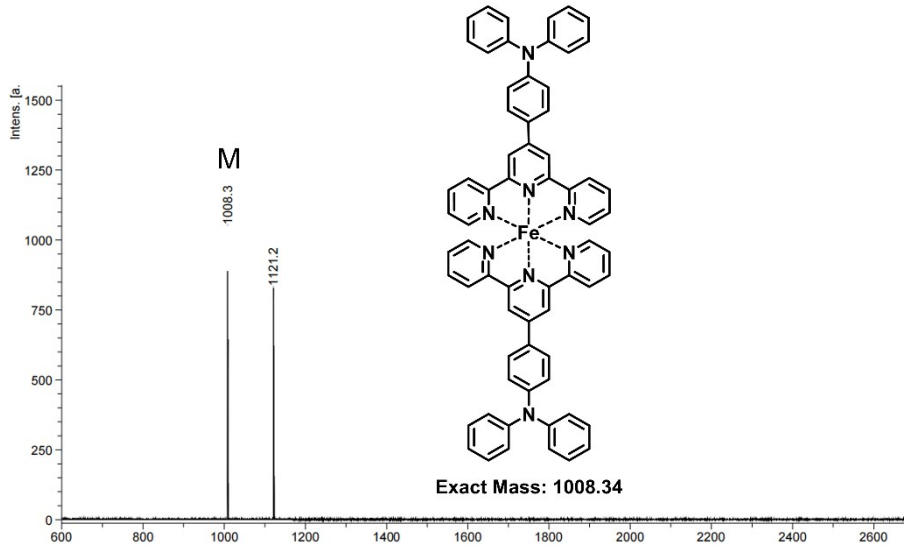

Fig. S34 MALDI-TOF mass spectrum of the Fe monomer in CH_3CN.

2. Supplemental Methods

General Characterizations. ^{1}H and ^{13}C nuclear magnetic resonance (NMR) spectra of the organic ligand and monomers were measured with a Bruker AV-500 spectrometer at 25 °C. Ultraviolet-visible (UV-vis) absorption spectra were recorded on a JASCO V-770 spectrophotometer at room temperature. atomic force microscopy (AFM) studies were carried out using a Bruker Dimension Icon AFM. Scanning electron microscopy (SEM) images were obtained using a Zeiss Sigma 300 high-resolution field emission scanning electron microscope (FE-SEM) with an accelerated voltage of 10 kV and accelerated current of 10 mA. SEM-EDS element mapping images were obtained by an Oxford Instruments Ultim Max 100 EDS detector with an accelerated voltage of 20 kV and an accelerated current of 15 mA. MALDI-TOF mass spectra were obtained using a Bruker Daltonics Autoflex III TOF. IR-RAS were obtained using a Bruker ALPHA II.

Metallopolymer Preparation. Electropolymerization was performed in CH_2Cl_2 containing 0.2 mM monomer and 0.1 M n-Bu_4NClO_4 with a CHI660E electrochemical analyzer in standard three-electrode system. ITO was the working electrode, the platinum foil was the counter electrode, and Ag/Ag^+ was the reference electrode. The Co and Fe metallopolymers were prepared through cyclic voltammetry (CV) from 0.2 V to 1.0 V at a scan rate of 50 mV/s on indium-tin oxide (ITO) glass electrodes by scanning 1–5 and 3–15 cycles (in increments of 1 and 3 cycles, respectively). After each scan, the ITO electrode was extracted from the monomer solution, rinsed with CH_2Cl_2 and then dried.

Memristive Test. The resistive switching was tested using an X-Tech series SAMJ module purchased from China VR (Xiamen) Technology Co., Ltd. The grounded eutectic gallium-indium (EGaIn) alloy tip was prepared as the top electrode[5,6]. The bias was applied to the bottom ITO electrode. The current signal was read through the top electrode by a logarithmic amplifier calibrated by a series of resistors (100 Ω–100 MΩ). The *J–V* curves were obtained by employing a cyclic linear bias scan while recording the corresponding current signals, with a scan rate of 500 mV/s. The write-read-erase *J–T* and corresponding *V–T* curves were obtained by manually switching to a constant bias and recording the corresponding current signals and time.

3. Supplemental Synthesis

Commercially available solvents and reagents were used without further purification.

Synthesis of the ligand 4'-(4-(diphenylamino)phenyl)-[2,2':6',2"]terpyridine

4'-(4-(diphenylamino)phenyl)-[2,2':6',2"]terpyridine was synthesized using the classical protocol of the Suzuki cross-coupling reaction[7]. To a round bottom flask with a magnetic stir bar was added 4'-bromo-2,2':6',2"-terpyridine (312 mg, 1.0 mmol, 1.0 equiv), 4-(diphenylamino)phenylboronic acid (318 mg, 1.1 mmol, 1.1 equiv), $Pd(PPh_3)_4$ (35 mg, 0.03 mmol, 0.03 equiv), Cs_2CO_3 (978 mg, 3.0 mmol, 3.0 equiv), THF (30 mL) and H_2O (5 mL). The reaction mixture was stirred and refluxed under argon atmosphere for 48 hours. After cooling to room temperature, the mixture was diluted with dichloromethane (30 mL) and washed with distilled water (3 × 20 mL). The organic layer was dried with Na_2SO_4, filtered, and concentrated. The crude product was

purified by silica gel column chromatography (eluting with 1:8:1 $CH_3OH/CH_2Cl_2/NH_4OH$) to yield 404 mg 4'-(4-(diphenylamino)phenyl)-[2,2':6',2"]terpyridine as a faint yellow solid (85% yield). ^{1}H NMR ^{1}H NMR (500 MHz, CD_2Cl_2) δ 8.64 (s, 2H), 8.62 (d, J = 4.9 Hz, 2H), 8.59 (d, J = 8.0 Hz, 2H), 7.81 (t, J = 7.7 Hz, 2H), 7.71 (d, J = 8.9 Hz, 2H), 7.28 (dd, J = 7.5, 4.7 Hz, 2H), 7.23 (t, J = 8.5, 7.5 Hz, 4H), 7.11 – 7.05 (m, 6H), 7.00 (t, J = 7.3 Hz, 2H). ^{13}C NMR (500 MHz, CD_2Cl_2) δ 156.34, 156.05, 149.61, 149.27, 149.06, 147.52, 136.93, 131.75, 129.52, 128.08, 125.06, 123.95, 123.62, 123.04, 121.19, 118.08, 29.83. MALDI-TOF: m/z calcd. for $[M]^+$ 476.20 found 476.2.

Synthesis of the Co monomer

Co monomer was synthesized using a two-step protocol[8]. To a round bottom flask with a magnetic stir bar was added the ligand 4'-(4-(diphenylamino)phenyl)-[2,2':6',2"]terpyridine (98 mg, 0.205 mmol, 2.05 equiv) and 10 mL CH_2Cl_2. After stirring until L was completely dissolved, a solution of $CoCl_2$ (13 mg, 0.1 mmol, 1.0 equiv) in methanol (5 mL) was added dropwise to the reaction mixture. The reaction mixture was stirred at room temperature under ambient condition for 15 minutes. The solvent was removed by rotary evaporation, and the mixture was dissolved with a small amount of methanol. The intermediate product was precipitated by adding saturated KPF_6 aq., filtered, and washed with H_2O, toluene and diethyl ether. Then, the precipitate was dissolved in 5 mL CH_3CN and excess $AgNO_3$ (85 mg, 0.5 mmol, 5.0 equiv) was added. The gray precipitate was removed by filtration and washed with CH_3CN until the filtrate was colorless. The filtrate was then concentrated in vacuo and saturated KPF_6 aq was added. The precipitate was filtered and washed with H_2O and diethyl ether. The crude product was dissolved in CH_2Cl_2 and purified by silica gel chromatography (eluting with 2:5 CH_3CN/CH_2Cl_2) to yield 76 mg Co monomer as a red solid (75% yield). ^{1}H NMR (500 MHz, CD_3CN) δ 9.14 (s, 4H), 8.67 (d, J = 8.0 Hz, 4H), 8.26 – 8.19 (m, 8H), 7.48 (t, J = 7.5 Hz, 8H), 7.44 – 7.38 (m, 8H), 7.34 – 7.27 (m, 12H), 7.26 (d, J = 8.9 Hz, 4H). ^{13}C NMR (500 MHz, CD_3CN) δ 157.22, 157.03, 156.17, 152.83, 146.76, 143.53, 131.18, 130.59, 130.25, 127.38, 127.04, 126.17, 126.13, 124.10, 120.65. MALDI-TOF: m/z calcd. for $[M]^+$ 1011.33 found 1011.3.

Synthesis of the Fe monomer

Fe monomer was synthesized using a one-step protocol[9]. To a round bottom flask with a magnetic stir bar was added the ligand 4'-(4-(diphenylamino)phenyl)-[2,2':6',2"]terpyridine (95 mg, 0.205 mmol, 2.05 equiv) and 10 mL CH_2Cl_2. After stirring until L was completely dissolved, a solution of $FeCl_2$ (12.5 mg, 0.1 mmol, 1.0 equiv) in 5 mL methanol was added dropwise to the reaction mixture. The reaction mixture was stirred at room temperature under ambient condition for 1 h. The solvent was removed by rotary evaporation and the mixture was dissolved with a small amount of methanol. The crude product was precipitated by adding saturated KPF_6 aq., filtered, washed with H_2O, toluene and diethyl ether. Then, the precipitate was dissolved in CH_2Cl_2 and purified by silica gel chromatography (eluting with 1:9 CH_3CN/CH_2Cl_2) to yield 81 mg Fe monomer as a deep purple solid (80% yield). ^{1}H NMR (500 MHz, CD_3CN) δ 9.12 (s, 4H), 8.58 (d, J = 7.9 Hz, 4H), 8.21 (d, J = 9.0 Hz, 4H), 7.89 (t, J = 7.8 Hz, 4H), 7.45 (t, J = 7.5 Hz, 8H), 7.31 (d, J = 8.5 Hz, 4H), 7.29 – 7.21 (m, 12H), 7.19 (d, J = 5.6 Hz, 4H), 7.07 (dd, J = 7.2, 5.6 Hz, 4H). ^{13}C NMR (500 MHz, CD_3CN) δ 160.69, 158.77, 153.65, 151.14, 150.26, 147.47, 139.19, 130.42, 129.34, 129.10, 127.74, 126.32, 125.25, 124.21, 122.13, 121.05. MALDI-TOF: m/z calcd. for $[M]^+$ 1008.34 found 1008.3.

4. Supplemental References

1 L. Schnaubelt, H. Petzold, J. M. Speck, T. Rüffer, G. Hörner and H. Lang, *Z. Für Anorg. Allg. Chem.*, 2018, **644**, 1257–1267.
2 S. Sun and A. J. Lees, *Inorg. Chem.*, 2001, **40**, 3154–3160.
3 G. Socrates, *J. Am. Chem. Soc.*, 2002, **124**, 1830.
4 B. B. Cui, Z. Mao, Y. Chen, Y. W. Zhong, G. Yu, C. Zhan and J. Yao, *Chem. Sci.*, 2015, **6**, 1308–1315.
5 J. Jang, P. He and H. J. Yoon, *Acc. Chem. Res.*, 2023, **56**, 1613–1622.
6 Y. Xie, Z. Cao, W. Peng and Y. Li, *Adv. Mater. Technol.*, 2025, **10**, e00674.
7 S. Guan, Z. Wei, N. Han, Y. Wei, B. Xu, M. Wang and J. Shi, *Chin. Chem. Lett.*, 2024, **35**, 109348.
8 J. A. Mann, J. Rodríguez-López, H. D. Abruña and W. R. Dichtel, *J. Am. Chem. Soc.*, 2011, **133**, 17614–17617.
9 C. W. Machan, M. Adelhardt, A. A. Sarjeant, C. L. Stern, J. Sutter, K. Meyer and C. A. Mirkin, *J. Am. Chem. Soc.*, 2012, **134**, 16921–16924.